Nuclear matter symmetry energy at 0.03⩽ρ/ρ_{0}⩽0.2

R. Wada *et al.*

Phys. Rev. C **85**, 064618 — Published 25 June 2012

DOI: 10.1103/PhysRevC.85.064618

The Nuclear Matter Symmetry Energy at $0.03 \leq \rho/\rho_0 \leq 0.2$

R. Wada,[1,2] K. Hagel,[2] L. Qin,[2] J. B. Natowitz,[2] Y. G. Ma,[3] G. Röpke,[4] S. Shlomo,[2] A. Bonasera,[2,5] S. Typel,[6] Z. Chen,[2,1] M. Huang,[2,1] J. Wang,[2,1] H. Zheng,[2] S. Kowalski,[7] C. Bottosso,[2] M. Barbui,[2] M. R. D. Rodrigues,[2] K. Schmidt,[2] D. Fabris,[8] M. Lunardon,[8] S. Moretto,[8] G. Nebbia,[8] S. Pesente,[8] V. Rizzi,[8] G. Viesti,[8] M. Cinausero,[9] G. Prete,[9] T. Keutgen,[10] Y. El Masri,[10] and Z. Majka[11]

[1]*Institute of Modern Physics HIRFL, Chinese Academy of Sciences, Lanzhou, 730000, China*
[2]*Cyclotron Institute, Texas A&M University, College Station, Texas 77843*
[3]*Shanghai Institute of Nuclear Research, Chinese Academy of Sciences, Shanghai 201800, China*
[4]*University of Rostock, FB Physik, Rostock, Germany*
[5]*Laboratori Nazionali del Sud, INFN, via Santa Sofia, 62, 95123 Catania, Italy*
[6]*GSI Helmholtzzentrum fur Schwerionenforschung GmbH, Theorie, Planckstraße 1, D-64291 Darmstadt, Germany*
[7]*Institute of Physics, Silesia University, Katowice, Poland.*
[8]*Dipartamento di Fisica dell Universita di Padova and INFN Sezione di Padova, Padova, Italy*
[9]*INFN Laboratori Nazionali di Legnaro, Legnaro, Italy*
[10]*FNRS and IPN, Université Catholique de Louvain, B-1348 Louvain-Neuve, Belgium*
[11]*Smoluchowski Institute of Physics, Jagiellonian University, Krakow, Poland*

Measurements of the density dependence of the Free symmetry energy in low density clustered matter have been extended using the NIMROD multi-detector at Texas A&M University. Thermal coalescence models were employed to extract densities, ρ, and temperatures, T, for evolving systems formed in collisions of 47 A MeV ^{40}Ar + ^{112}Sn ,^{124}Sn and ^{64}Zn + ^{112}Sn , ^{124}Sn. Densities of $0.03 \leq \rho/\rho_0 \leq 0.2$ and temperatures in the range 5 to 10 MeV have been sampled. The Free symmetry energy coefficients are found to be in good agreement with values calculated using a quantum statistical model. Values of the corresponding symmetry energy coefficient are derived from the data using entropies derived from the model.

PACS numbers: 25.70.Pq
Keywords: Intermediate Heavy ion reactions, chemical equilibrium, neutron and proton chemical potential, quantum statisitcal model calculations

I. I. INTRODUCTION

The symmetry energy of nuclear matter is a fundamental ingredient in the investigation of nuclear and astrophysical phenomena. The symmetry energy characterizes the dependence of the nuclear binding energy on the asymmetry $\delta = (N - Z)/A$ where Z and N are the proton and neutron numbers, and $A = N + Z$. As a general representation of the symmetry energy coefficient we use the definition

$$E_{\rm sym}(\rho, T) = \frac{1}{2}\big(E(\rho, 1, T) + E(\rho, -1, T)\big) - E(\rho, 0, T) \quad (1)$$

where $E(\rho, \delta, T)$ is the energy per nucleon of nuclear matter with density ρ, asymmetry δ, and temperature T. If a quadratic dependence is assumed this definition becomes identical to the frequently used alternative of taking the second derivative of $E(\rho, \delta, T)$ with respect to the asymmetry $\delta = 0$. Our empirical knowledge of the symmetry energy near the saturation density, ρ_0, is based primarily on the binding energies of nuclei. The Bethe-Weizsäcker mass formula leads to values of about $E_{\rm sym}(\rho_0, 0) = 28 - 34$ MeV for the symmetry energy at zero temperature and saturation density $\rho_0 = 0.16$ fm^{-3}, if surface asymmetry effects are properly taken into account [1]. In contrast to the value of $E_{\rm sym}(\rho_0, 0)$, the variation of the symmetry energy with density and temperature is intensely debated. Many experimental and theoretical investigations have been performed to estimate the behavior of the symmetry energy as a function of ρ and T. Recent reviews are given by Li *et al.* [2] and by Lattimer and Lim [3].

In the Fermi energy domain symmetry energy effects have been investigated using judiciously chosen observables from nuclear reactions [2–7]. In the theoretical investigations quasiparticle approaches such as the Skyrme Hartree-Fock and relativistic mean field (RMF) models or Dirac-Brueckner Hartree-Fock (DBHF) calculations are used [2, 8, 9]. In such calculations the symmetry energy tends to zero in the low-density limit for uniform matter. However, in accordance with the mass action law, cluster formation dominates the structure of low-density symmetric matter at low temperatures. Thus at low density the symmetry energy changes mainly because additional binding is gained in symmetric matter due to formation of clusters and pasta structures [10]. As a result the symmetry energy in this low-temperature limit has to be equal to the binding energy per nucleon associated with the strong interaction of the most bound nuclear cluster. A single-nucleon quasiparticle approach cannot account for such structures. The correct low-density limit can be recovered only if the formation of clusters is properly taken into account, as has previously been shown in [11] in the context of a virial expansion valid at very low densities and in Ref. [12]. Since, at

low density, the symmetry energy changes mainly because additional binding is gained in the formation of clusters [11, 13–16], measurements of nucleon and light cluster emission from the participant matter which is produced in near Fermi energy heavy ion collisions can be employed to probe the EOS at low density and moderate temperatures where clustering is important [13, 14]. Our previous data demonstrated a large degree of alpha clustering for densities at and below ~ 0.05 times normal nuclear density, ρ_0 (0.16 nucleons/fm^3) and temperatures of 4 to 10 MeV. Using these data we derived symmetry energy coefficients in low density nuclear matter [13, 14]. The analysis employed the isoscaling technique which compares yields for two systems with similar temperatures but different N/Z ratios to determine the differences in chemical potentials and symmetry energy [17, 18]. The NIMROD 4π multi-detector at Texas A & M University has now been used to extend our measurements to higher densities. Cluster production in collisions of 47 A MeV ^{40}Ar with ^{112,124}Sn and ^{64}Zn with ^{112,124}Sn was studied. We report here determinations of symmetry energy coefficients at $0.03 \leq \rho/\rho_0 \leq 0.2$ and moderate temperatures. Our results for this expanded range of densities are in reasonable agreement with those of a quantum statistical model calculation incorporating medium modifications of the cluster binding energies [12, 19, 20].

II. EXPERIMENTAL TECHNIQUES

The experiments were performed using beams from the K500 Superconducting Cyclotron at the Texas A&M University Cyclotron Institute, incident on targets in the NIMROD detector. NIMROD consists of a 166 segment charged particle array set inside a neutron ball [21]. The charged particle array is arranged in 12 rings of Si-CsI telescopes or single CsI detectors concentric around the beam axis. The CsI detectors are 1-10 cm thick Tl doped crystals read by photomultiplier tubes. A pulse shape discrimination method is employed to identify light particles in the CsI detectors. For this experiment each of the forward rings included two segments having two Si detectors (150 and 500 μm thick) in front of the CsI detectors (super telescopes) and three having one Si detector (300 μm thick). Each super telescope was further divided into two sections. Neutron multiplicity was measured with the 4π neutron detector surrounding the charged particle array. This detector is a neutron calorimeter filled with gadolinium doped pseudocumene. Thermalization and capture of emitted neutrons in the ball leads to scintillation light which is observed with phototubes providing event by event determinations of neutron multiplicity. Further details on the detection system, energy calibrations and neutron ball efficiency may be found in references [22, 23]. The combined neutron and charged particle multiplicities were employed to select the most violent events for subsequent analysis.

III. ANALYSIS

The dynamics of the collision process allow us to probe the nature of the intermediate velocity "nucleon-nucleon" emission source [13, 14, 22, 23]. Measurement of emission cross sections of nucleons and light clusters together with suitable application of a coalescence ansatz [24] provides the means to probe the properties and evolution of the interaction region. The techniques used in the analysis have been detailed in several previous publications [13, 14, 22, 23] and are described briefly below. A notable difference from Refs. [13] and [14] is the method of density extraction. This is discussed more extensively in the following. We emphasize that the event selection is on the more violent collisions. Cross section weighting favors mid-range impact parameters.

An initial estimation of emission multiplicities at each stage of the reaction was made by fitting the observed light particle spectra assuming contributions from three sources, a projectile-like fragment (PLF) source, an intermediate velocity (IV) source, and a target-like fragment (TLF) source. A reasonable reproduction of the observed spectra is achieved. Except for the most forward detector rings the data are dominated by particles associated with the IV and TLF sources. The IV source velocities are very close to 50% of the beam velocity as seen in many other studies [22, 23]. The observed spectral slopes reflect the evolution dynamics of the source, not its internal temperature [25, 26]. For further analysis, this IV source is most easily sampled at the intermediate angles where contributions from the other sources are minimized. For the analysis of the evolution of the source we have selected the data in ring 9 of the NIMROD detector. This ring covered an angular range in the laboratory of 38° to 52°. An inspection of invariant velocity plots constructed for each ejectile and each system, as well as of the results of the three-source fit analyses, indicates that this selection of angular range minimizes contributions from secondary evaporative decay of projectile like or target like sources. We treat the IV source as a nascent fireball created in the participant interaction zone. The expansion and cooling of this zone leads to a correlated evolution of density and temperature which we probe using particle and cluster observables, yield, energy and angle.

A. Temperature

As in some previous work [13, 14] we have employed double isotope yield ratios [27, 28] to characterize the temperature at a particular emission time. For particles emitted from a single source of temperature, T, and having a volume Maxwellian spectrum the HHe double isotope yield ratio evaluated for particles of equal $v_{\rm surf}$ is $\sqrt{9/8}$ times the ratio derived from either the integrated particle yields or the yields at a given energy above the

barrier,

$$T_{\rm HHe} = \frac{14.3}{\ln\left(\sqrt{9/8}(1.59\ R_{v_{\rm surf}})\right)}. \qquad (2)$$

If Y represents a cluster yield, $R_{v_{\rm surf}} = Y(^2{\rm H})Y(^4{\rm He})/Y(^3{\rm H})Y(^3{\rm He})$ for clusters with the same surface velocity. The constants 14.3 and 1.59 reflect binding energy, spin, masses and mass differences of the ejectiles. Eq. (2) differs from the usual formulation only by the factor of $\sqrt{9/8}$ appearing in the logarithm term in the denominator.

Model studies [29] comparing Albergo model [27] temperatures and densities to the known input values have shown the double isotope ratio temperatures to be relatively robust in this density range. However the densities extracted using the Albergo relationships are useful only at the very lowest densities. Consequently, in this study we have employed a different means of density extraction – the thermal coalescence model of Mekjian [24].

B. Density

To determine the coalescence parameter P_0, the radius in momentum space, from our data we have followed the Coulomb corrected coalescence model formalism of Awes *et al.* [30] and previously employed by us in Ref. [23]. In the laboratory frame the derived relationship between the observed cluster and proton differential cross sections is

$$\frac{d^2N(Z,N,E_A)}{dE_A\,d\Omega} = R_{np}^N \frac{1}{N!Z!A}\left(\frac{4\pi P_0^3}{3[2m^3(E-E_C)]^{1/2}}\right)^{A-1} \times \left(\frac{d^2N(1,0,E)}{dE\,d\Omega}\right)^A, \qquad (3)$$

where the double differential multiplicity for a cluster of mass number A containing Z protons and N neutrons and having a Coulomb-corrected energy E_A, is related to the proton double differential multiplicity at the same Coulomb corrected energy per nucleon, $E - E_C$, where E_C is the Coulomb barrier for proton emission. R_{np} is the neutron to proton ratio.

Application of the coalescence model requires knowledge of cluster, neutron and proton differential cross sections with proper absolute normalizations. In this work absolute measured multiplicities for the selected violent events are employed. The neutron spectra are not measured. However, since within the framework of the coalescence model the yield ratios of two isotopes that differ by one neutron are determined by their binding energies and the n/p ratio in the coalescence volume, we have used the observed triton to ^{3}He yield ratio to derive the n/p ratio used in this analysis. Because our goal was to derive information on the density and temperature evolution of the emitting system, our analysis was not limited to determining an average P_0 value. Instead, as in our previous studies [13–15, 22, 23], results for d, t, ^{3}He, and ^{4}He were derived as a function of the surface velocity in the intermediate velocity source frame, i.e., the velocity of the emerging particle at the nuclear surface, prior to Coulomb acceleration. Results for the reaction of ^{40}Ar + ^{112}Sn are presented in Fig. 1. Values of P_0 for the other reactions are very similar. The low velocity cut off is imposed to avoid significant contamination from particles evaporated from the TLF source. The velocity of 6.6 cm/ns in the IV frame corresponds to the beam velocity and the rise in P_0 seen in the Figure indicates that these high velocity particles may not be amenable to an equilibrium treatment.

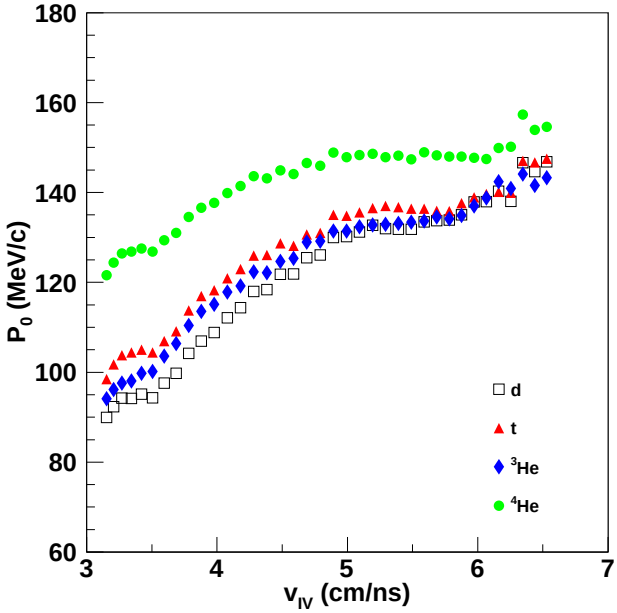

FIG. 1: (Color online) Coalescence parameters, P_0 as a function of surface velocity in the intermediate velocity source frame. Reaction: 47 A MeV ^{40}Ar + ^{112}Sn

In the Mekjian model thermal and chemical equilibrium determines coalescence yields of all species. Under these assumptions there is a direct relationship between the derived radius in momentum space and the volume of the emitting system. In terms of the P_0 derived from Eq. (3) and assuming a spherical source,

$$V = \frac{3h^3}{4\pi P_0^3}\left[\frac{Z!N!A^3}{2^A}(2s+1)e^{\frac{E_0}{T}}\right]^{\frac{1}{A-1}}, \qquad (4)$$

where h is Plancks constant, and Z, N, and A are the same as in Eq. (3), E_0 is the ground state binding energy, s the spin of the emitted cluster, and T is the temperature. Thus the volume can be derived from the observed P_0 and temperature values assuming a spherical source. We note that this volume is a free volume. From the relevant P_0 values we then determined volumes using Eq. (4).

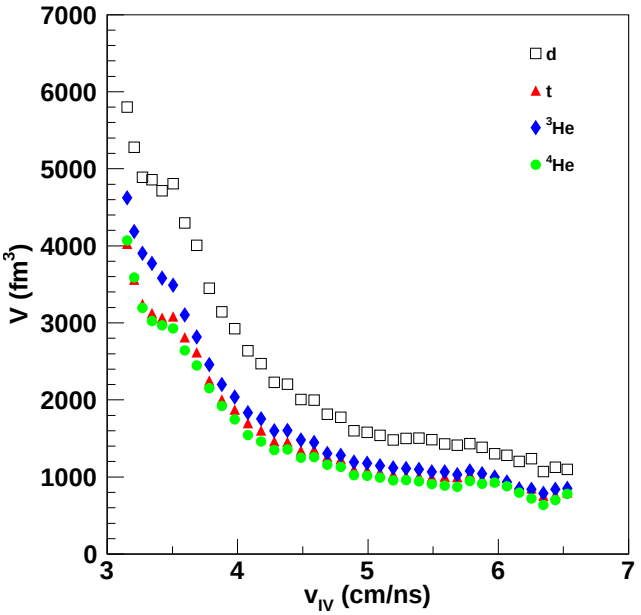

FIG. 2: (Color online) Coalescence model volumes as a function of velocity in the intermediate velocity source frame. Reaction: 47 A MeV ^{40}Ar + ^{112}Sn

See Fig. 2 where, again, results for the reaction ^{40}Ar + ^{112}Sn are presented.

A comparison of these volumes indicates good agreement for t, ^{3}He and ^{4}He. Volumes derived from the deuteron data are typically somewhat larger. This larger apparent volume for deuterons appears to reflect the fragility of the deuteron and its survival probability once formed [31]. For this reason we have used average volumes derived from the $A \geq 3$ clusters to calculate the densities. Given that mass is removed from the system during the evolution, we determined the relevant masses for each volume by assuming that the initial mass of the source was that obtained from the source fitting analysis and then deriving the mass remaining at a given $v_{\rm surf}$ from the observed energy spectra. This is also an averaging process and ignores fluctuations. Once these masses were known they were used to determine an excluded volume for the particles. Addition of this excluded volume to the free volume produced the total volumes needed for the density calculations. These were determined by dividing the remaining masses by the total volume. This was done as a function of $v_{\rm surf}$. This excluded volume correction is small for low $v_{\rm surf}$ but increases with increasing $v_{\rm surf}$. Densities are those of total number of nucleons, including the nucleons bound in clusters, per fm^3.

IV. RESULTS

A. Temperatures and Densities

Inspection of the results for the four different systems studied revealed that, as a function of surface velocity, the temperatures, densities and equilibrium constants for all systems are the same within statistical uncertainties. This indicates that the time evolution of the systems studied is very similar [23, 32]. Therefore we have combined values from all systems to determine the temperatures and densities reported in this paper.

We present in Fig. 3 the experimentally derived density and temperature evolution for the IV source. Estimated errors on the temperatures are 10% at low density evolving to 15% at the higher densities. In deriving our results we have invoked the correlation between average surface velocity and emission time for the early emitted particles on which we focus our attention. This is seen clearly in transport model calculations [32]. It is certainly true that density and temperatures corresponding to the different surface velocity bins are weighted averages over the underlying distributions. There will be fluctuations in T and ρ present at the time of particle emission. We assume these to be symmetric about the most probable value. There will then be additional fluctuations induced by mixing. Using the AMD model of Ono, and assuming at each time a single (time-decreasing) temperature we estimate that, for the higher surface velocities, the weighted average temperatures are $\leq 10\%$ lower than the input temperatures. This effect decreases at lower surface velocities where the rate of decrease of temperature with velocity is less. These estimates are included in our estimates of the temperature uncertainty. The error in the derivation of the density arises from the uncertainty on the volume which is dominated by the uncertainty in temperature and the uncertainty in source mass derived from source fitting to complex spectra. The estimated errors on the densities are $\pm 17\%$.

B. Isoscaling

Considering only bulk properties of homogeneous nuclear matter, and the standard thermodynamic relations that relate the Free energy, the Internal energy, and the entropy, as a function of ρ, δ, T we can expand with respect to δ to define the corresponding expressions for $F_{\rm sym}(\rho, T)$ and $S_{\rm sym}(\rho, T) = -\partial F_{\rm sym}(\rho, T)/\partial T$. This is analogous to the expressions given above for $E_{\rm sym}(\rho, T)$

The isoscaling technique has been used to derive information on $F_{\rm sym}$, the symmetry Free energy of the system. The isoscaling technique consists of measuring cluster yield ratios for two different excited systems (denoted by the index 1 and 2), having the same temperature (and density) and the same atomic number but differing in the Z/A ratio. For such systems liquid drop model binding energy terms other than those related to the symmetry

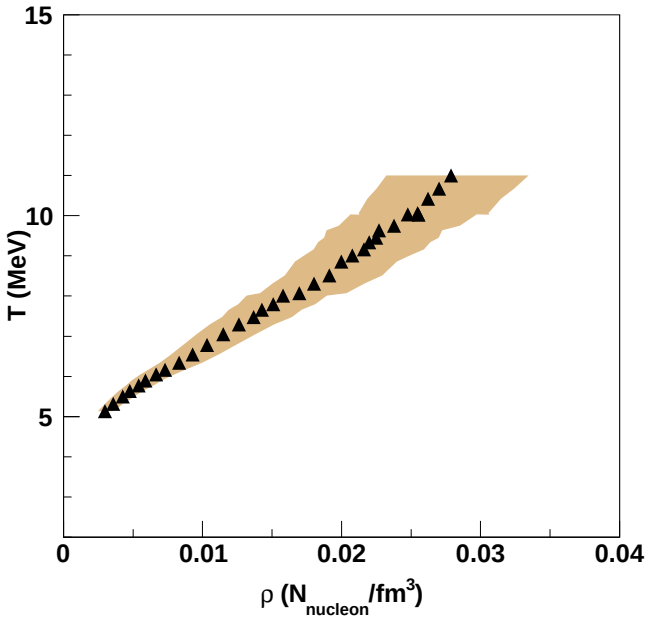

FIG. 3: (Color online) Temperatures and densities sampled by cluster emission from the expanding IV source.

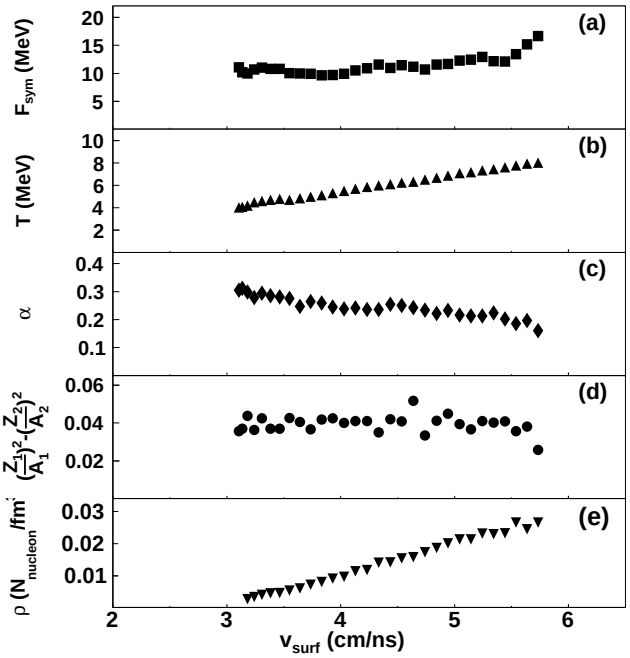

FIG. 4: Parameters of the analysis. (a) Symmetry Free energy coefficient, (b) Temperature, (c) Isoscaling parameter, α, (d) $(\frac{Z_1}{A_1})^2 - (\frac{Z_2}{A_2})^2$, (e) Density

energy coefficient essentially cancel and one can write [17, 18].

$$\frac{Y_2}{Y_1} = Ce^{((\mu_2(n)-\mu_1(n))N+(\mu_2(p)-\mu_1(p))Z)/T} = Ce^{\alpha N+\beta Z} \quad (5)$$

where C is a constant and $\mu(n)$ and $\mu(p)$ are the neutron and proton chemical potentials. The isoscaling parameters $\alpha = \big(\mu_2(n) - \mu_1(n)\big)/T$ and $\beta = \big(\mu_2(p) - \mu_1(p)\big)/T$, representing the difference in chemical potential between the two systems, may be extracted from suitable plots of yield ratios. Either parameter may then be related to the symmetry Free energy, $F_{\rm sym}$. We take the α parameter, which is expected to be less sensitive to residual Coulomb effects. Addressing specifically the symmetry Free energy and adopting the usual convention that system 2 is richer in neutrons than system 1, one can write

$$\alpha = 4F_{\rm sym}\left[\left(\frac{Z_1}{A_1}\right)^2 - \left(\frac{Z_2}{A_2}\right)^2\right]/T\,, \quad (6)$$

where Z is the atomic number and A is the mass number of the emitter [14, 17, 18]. Thus, $F_{\rm sym}$ may be derived directly from determinations of system temperatures, Z/A ratios, and isoscaling parameters. We emphasize that the present analysis is carried out for light species characteristic of the nuclear gas rather than, as in most previous analyses, for the intermediate mass fragments thought to be characteristic of the nuclear liquid. In this work we employ Eq. (5) with experimentally determined isoscaling parameters, α, temperatures, T, and Z/A ratios to determine the symmetry Free energy coefficient, $F_{\rm sym}$.

Fig. 4 (a-e) presents the results of our isoscaling analysis. The experimentally derived evolution of density, temperature, $[(Z_1/A_1)^2-(Z_2/A_2)^2]$, the isoscaling parameter α, and the Free symmetry energy coefficient are presented as a function of surface velocity in the IV frame. The correlations between these parameters become apparent in this figure. For the determination of the Free symmetry energies we have restricted ourselves to isoscaling results leading to alpha parameters with less than 15 % uncertainties. This restricts the temperature and density range for which the Free symmetry energies are reported in figure 4.

We see that T and ρ increase with increasing $v_{\rm surf}$. At the same time there is a decline in the isoscaling coefficient α. Combined, the terms of Eq. (5) lead to values of $F_{\rm sym}$ that rise gently with $v_{\rm surf}$.

C. Free Symmetry Energy

In Figure 5 the Free symmetry energy coefficients determined from the isoscaling analysis are plotted. Also shown are calculated Free symmetry energy coefficients obtained from a quantum statistical approach that includes medium modifications of the cluster binding energies [12, 15, 16, 19, 20]. A few-body Schrödinger equation has been solved that contains single-particle self-energy shifts as well as Pauli blocking factors. For given T and μ_p, μ_n, the nucleon density is calculated. To obtain a thermodynamic potential, the Free energy as function of

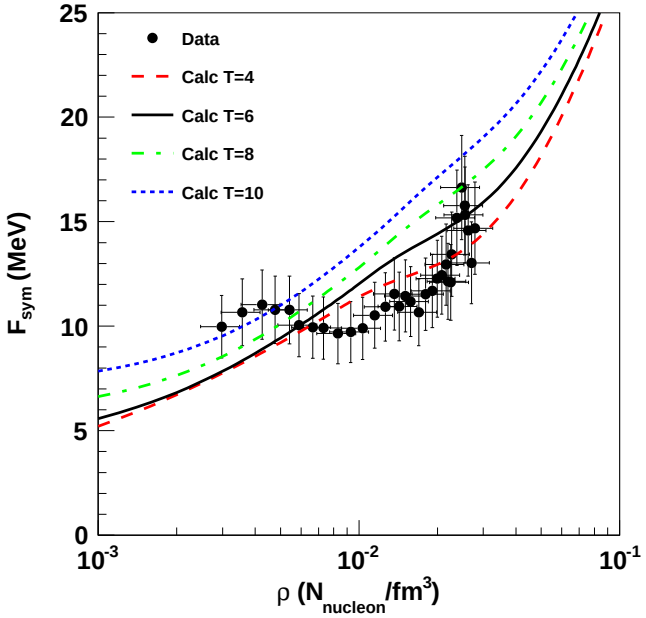

FIG. 5: (Color online) Free symmetry energy *vs.* density. Symbols show experimental points. Lines are calculated values for T =4, 6, 8 and 10 MeV [12, 15, 16, 19, 20]

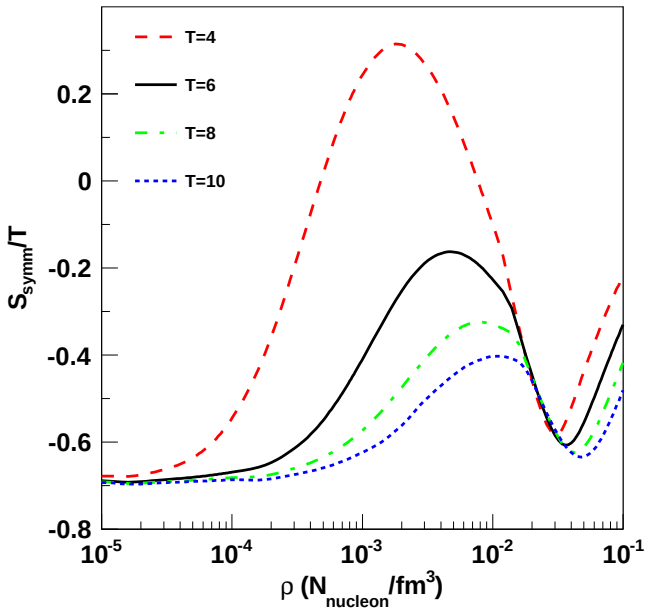

FIG. 6: (Color online) Symmetry entropy vs density. Symbols show experimental points and lines show calculations for T=4, 6, 8 and 10 MeV.

T, n_n, n_p is evaluated by integration. The further thermodynamic quantities are determined from the Free energy in a consistent way.

Isotherms of the Free symmetry energy at T = 4, 6, 8 and 10 MeV are also shown in Fig. 5. Note that the experimental data correspond to changing temperatures as seen in Fig. 4. Within the error bars, the general behavior of the experimental data is fairly well reproduced by the calculations. The data are somewhat below the calculated values, in particular in the intermediate region.

To derive the values of the Internal symmetry energy from the Free symmetry energy, the symmetry entropy must be known. The calculations of the symmetry entropies have been performed using the model of Typel *et al.* [12] where the Free energy, the Internal energy and the entropy have been given for symmetric matter. For pure neutron matter, the RMF approach can be used because there is no cluster formation.

We calculated the entropy within the QS approach by differentiating the Free energy with respect to the temperature. In Figure 6 we present the symmetry entropy, i.e. the difference between the entroy of neutron matter and that of symmetric matter, for different temperatures using the recent quantum statistical calculations of momentum dependent energy shifts of light clusters [16].

In contrast to the mixing entropy that leads to a larger entropy for uncorrelated symmetric matter in comparison with pure neutron matter, the formation of correlations, in particular clusters, will reduce the entropy in symmetric matter, see also Fig. 9 of Ref. [12]. For parameter

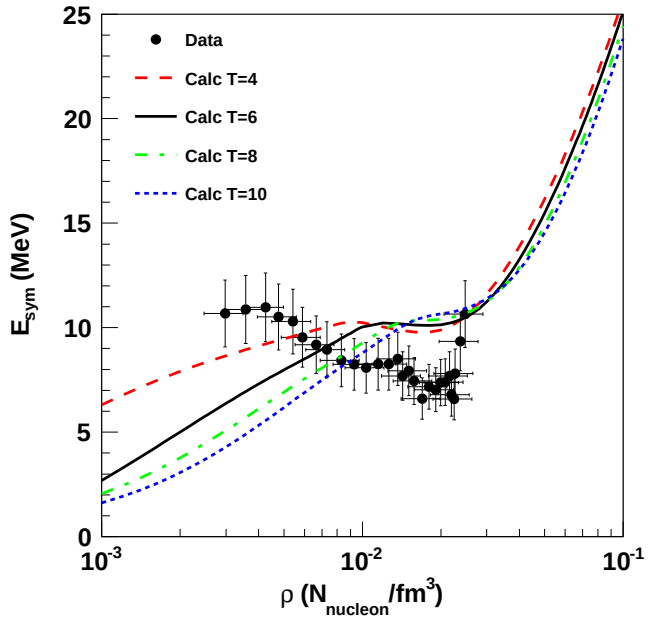

FIG. 7: (Color online) Symmetry energy vs density. Symbols show experimental points and lines show calculations for T=4, 6, 8 and 10 MeV.

values for which the yields of free nucleons in symmetric matter are small, the symmetry entropy may become positive. The fraction of nucleons bound in clusters can decrease due to increasing temperature or the dissolution of bound states at high densities due to the Pauli blocking. Then, the symmetric matter recovers its larger entropy so that the symmetry entropy becomes negative.

The corresponding results for the symmetry energy are shown in Fig. 7. Experimental as well as calculated values indicate a large value of the symmetry energy also in the low-density region since the alpha-fraction in symmetric matter becomes large at low temperatures, and the value of the binding energy per nucleon determines the Internal energy. This effect in not included in quasiparticle approaches such as standard relativistic mean field calculations because few-body correlations are neglected.

V. SUMMARY AND CONCLUSIONS

The NIMROD multi-detector at Texas A&M University has been employed to extend our earlier measurements of symmetry energy coefficients in low density clustered nuclear matter. Yields of light particles produced in the collisions of 47 A MeV ^{40}Ar with ^{112}Sn ,^{124}Sn and ^{64}Zn with ^{112}Sn, ^{124}Sn were employed in Thermal coalescence model analyses to derive densities and temperatures of the evolving emitting systems. Isoscaling analyses were used to determine the Free symmetry energies of these systems. Comparisons of the experimental values are made with those of calculations made using a model which incorporates medium modifications of cluster binding energies. The model calculated symmetry entropies have been used together with the experimental Free symmetry energies to derive symmetry energies of nuclear matter at densities of $0.03 \leq \rho/\rho_0 \leq 0.2$ and temperatures in the range 5 to 10 MeV.

VI. ACKNOWLEDGEMENTS

This work was supported by the United States Department of Energy under Grant # DE-FG03- 93ER40773 and by The Robert A. Welch Foundation under Grant # A0330.

[1] P. Danielewicz, Nucl. Phys. **A727**, 233 (2003).
[2] B. A. Li *et al.*, Phys. Rep. **464**, 113 (2008).
[3] J. M. Lattimer and Y. Lim, ArXiv: 1203.4286v1 [nucl-th] (2012).
[4] V. Baran, *et al.*, Phys. Rep. **410**, 335 (2005).
[5] M. B. Tsang *et al.*, Phys. Rev. Lett. **102**, 122701 (2009).
[6] D. V. Shetty, S. J. Yennello, and G. A. Souliotis, Phys. Rev. C **76**, 024606 (2007).
[7] C. Sfienti, *et al.*, Phys. Rev. Lett. **102**, 152701 (2009).
[8] M. DiToro *et al.*, J. Phys. G **37**, 083101 (2010).
[9] F. Sammarruca, J. Mod. Phys. E **19**, 1259 (2010).
[10] G.Watanabe, *et al.*, Phys. Rev. Lett. **103**, 121101 (2009).
[11] C. J. Horowitz and A. Schwenk, Nucl. Phys. **A776**, 55 (2006).
[12] S. Typel, G. Röpke, T. Klähn, D. Blaschke and H. H. Wolter, Phys. Rev. C **81**, 015803 (2010).
[13] S. Kowalski *et al.*, Phys. Rev. C **75** 014601 (2007).
[14] J. B. Natowitz *et al.*, Phys. Rev. Lett. **104**, 202501 (2010)
[15] G. Röpke, Phys. Rev. C **79**, 014002 (2009)
[16] G. Röpke, arXiv:1101.4685v2, Nucl. Phys. **A867**, 66 (2011).
[17] M. B. Tsang *et al.*, Phys. Rev.C **64**, 041603 (2001)
[18] S. R. Souza *et al.*, Phys. Rev. C **78**, 014605 (2008).
[19] K. Sumiyoshi *et al.*, Astron. Astrophys **303**, 475 (1995).
[20] C. Kuhrts *et al.*, Phys. Rev. C **63**, 034605 (2001).
[21] S. Wuenschel *et al.*, Nucl. Instrum. Methods Phys. Res. **A604**, 578 (2009).
[22] L. Qin, Thesis, Texas A&M University (2008).
[23] K. Hagel *et al.*, Phys. Rev. C **62**, 034607 (2000).
[24] A.Z. Mekjian, Phys. Rev. C **17**, 1051 (1978); Phys. Rev. Lett. **38**, 640 (1977).
[25] W. Bauer, Phys. Rev. C **51**, 803 (1995).
[26] H. Zheng *et al.*, Phys. Lett. **B696**, 178 (2011).
[27] S. Albergo *et al.*, Nuovo Cimento **A89**, 1 (1985).
[28] A. Kolomiets, V. M. Kolomietz, and S. Shlomo, Phys. Rev. C **55**, 1376 (1997)
[29] S. Shlomo *et al.*, Phys. Rev. C **79** , 034604 (2009).
[30] T. C. Awes *et al.*, Phys. Rev. C **24**, 89(1981)
[31] I. Cervesato, *et al.*, Phys. Rev. C **45**, 2369 (1992).
[32] J. Wang *et al.*, Phys. Rev. C **72**, 024603 (2005).